

Epitopes Displayed in a Cyclic Peptide Scaffold Bind SARS-CoV-2 Antibodies

Camilla Eriksson,^[a] Sunithi Gunasekera,^[a] Taj Muhammad,^[a] Mingshu Zhang,^[a] Ida Laurén,^[b] Sara M Mangsbo,^[b] Martin Lord,^[b] and Ulf Göransson^{*,[a]}

The SARS-CoV-2 virus that causes COVID-19 is a global health issue. The spread of the virus has resulted in seven million deaths to date. The emergence of new viral strains highlights the importance of continuous surveillance of the SARS-CoV-2 virus by using timely and accurate diagnostic tools. Here, we used a stable cyclic peptide scaffolds to present antigenic sequences derived from the spike protein that are reactive to SARS-CoV-2 antibodies. Using peptide sequences from different

domains of SARS-CoV-2 spike proteins, we grafted epitopes on the peptide scaffold sunflower trypsin inhibitor 1 (SFTI-1). These scaffold peptides were then used to develop an ELISA to detect SARS-CoV-2 antibodies in serum. We show that displaying epitopes on the scaffold improves reactivity overall. One of the scaffold peptides (S2_1146-1161_c) has reactivity equal to that of commercial assays, and shows diagnostic potential.

Introduction

Severe acute respiratory disease coronavirus 2 (SARS-CoV-2) is a beta-type coronavirus that causes COVID-19.^[1] Originating in Wuhan, China, in December 2019^[2,3] SARS-CoV-2 spread to cause a worldwide pandemic with devastating consequences for global human health. New viral strains have emerged (e.g. alpha, beta, delta, gamma, and omicron variants), and others are still being discovered, which highlights the necessity for efficient diagnostics, therapeutics, and the continuous development of new vaccines. SARS-CoV-2 belongs to the same family as SARS-CoV and Middle East respiratory syndrome (MERS).^[4] SARS-CoV-2 shares 79.6% sequence similarity to SARS-CoV^[5] that caused a previous outbreak in the years 2002–2004.^[6,7] Both SARS-CoV and Sars-CoV-2 target the angiotensin converting enzyme (ACE-2) receptor on host cells.^[8]

SARS-CoV-2 consists of four major structural proteins, spike (S), membrane (M), envelope (E), and nucleocapsid (N) proteins.^[9] The focus of the research and serological analysis has been on the spike (S) glycoprotein as it is located on the surface of the SARS-CoV-2, where it mediates viral entry into host cells and is a potent target for neutralizing antibodies.^[10] Specifically, several reports support that neutralizing antibodies are produced to potentially disrupt the interaction between

receptor binding domain (RBD) and ACE2 receptor, during a SARS-CoV infection.^[11,12] Common spike protein antigenic regions include the full-length spike, the spike regions S1 and S2^[13,14] and the receptor binding domain (RBD).

The aim of the current work was to determine whether cyclic scaffold peptides grafted with truncated sequences of 10–15 amino acids from immunogenic regions of the spike protein could be used in the diagnosis of COVID-19. These peptides might have certain advantages over the antigens in use today. RBD, S1, and S2 require cell expression systems, which are expensive and time-consuming. With the rapid emergence of new variants, the serological analysis tools need to be updated frequently, thus more cost- and time-effective tools are desirable. Our scaffold peptides are produced by solid-phase peptide synthesis, a method that provides a cost-efficient way to rapidly produce new antigens. It is also more flexible as new sequences (or modifications in sequences as required) can be produced quickly to combat rapidly evolving SARS-CoV-2 strains. Furthermore, short antigenic regions give the potential opportunity to resolve fine specificities in COVID-19 antibody profiles and to understand their impact.^[15] Information on antibody profiles can give valuable insight into heterogeneity observed in clinical symptoms, for example, variable disease severity observed among COVID-19 patients. This information can benefit epidemiology studies to predict the likely path to recovery of a patient and suggest potential medical interventions needed to ensure complete recovery.

Small cyclic peptides or miniproteins with exceptional stability have proven useful in drug design to stabilize epitopes of interest. Among them, the cyclotides,^[16–20] sunflower trypsin inhibitor-1 (SFTI-1)^[21–34] and rhesus theta defensins^[35] represent well-studied peptide families. SFTI-1 is a 14-residue potent trypsin inhibitor found in the seeds of the common sunflower.^[21] It has a cyclic peptide backbone, and two cysteines forming a single disulfide between two β -sheet strands. SFTI-1 is remarkably stable against enzymatic degradation.^[36] SFTI-1 has two loops, a structural loop and a trypsin inhibitory loop,

[a] C. Eriksson, Prof. S. Gunasekera, Dr. T. Muhammad, M. Zhang, Prof. U. Göransson
Department of Pharmaceutical Biosciences
Uppsala University
Biomedical Centre, Box 591, 75123 Uppsala (Sweden)
E-mail: ulf.goransson@farmbio.uu.se

[b] I. Laurén, Prof. S. M Mangsbo, Dr. M. Lord
Department of Pharmacy, Uppsala University
Biomedical Centre, 75123, Uppsala (Sweden)

Supporting information for this article is available on the WWW under <https://doi.org/10.1002/cbic.202300103>

© 2023 The Authors. ChemBioChem published by Wiley-VCH GmbH. This is an open access article under the terms of the Creative Commons Attribution License, which permits use, distribution and reproduction in any medium, provided the original work is properly cited.

and most importantly, the latter has been shown to be amenable to epitope grafting.^[37] This includes one example where SFTI-1 stabilized an immunogenic epitope protruding from the fibrinogen protein.^[29]

Herein, we synthesized linear peptide epitopes and epitopes grafted on peptide scaffolds for the development of a SARS-CoV-2 ELISA (Figure 1). We used antigenic peptide epitopes from SARS-CoV-2 spike protein;^[38] S1, RBD, (C-terminal region,

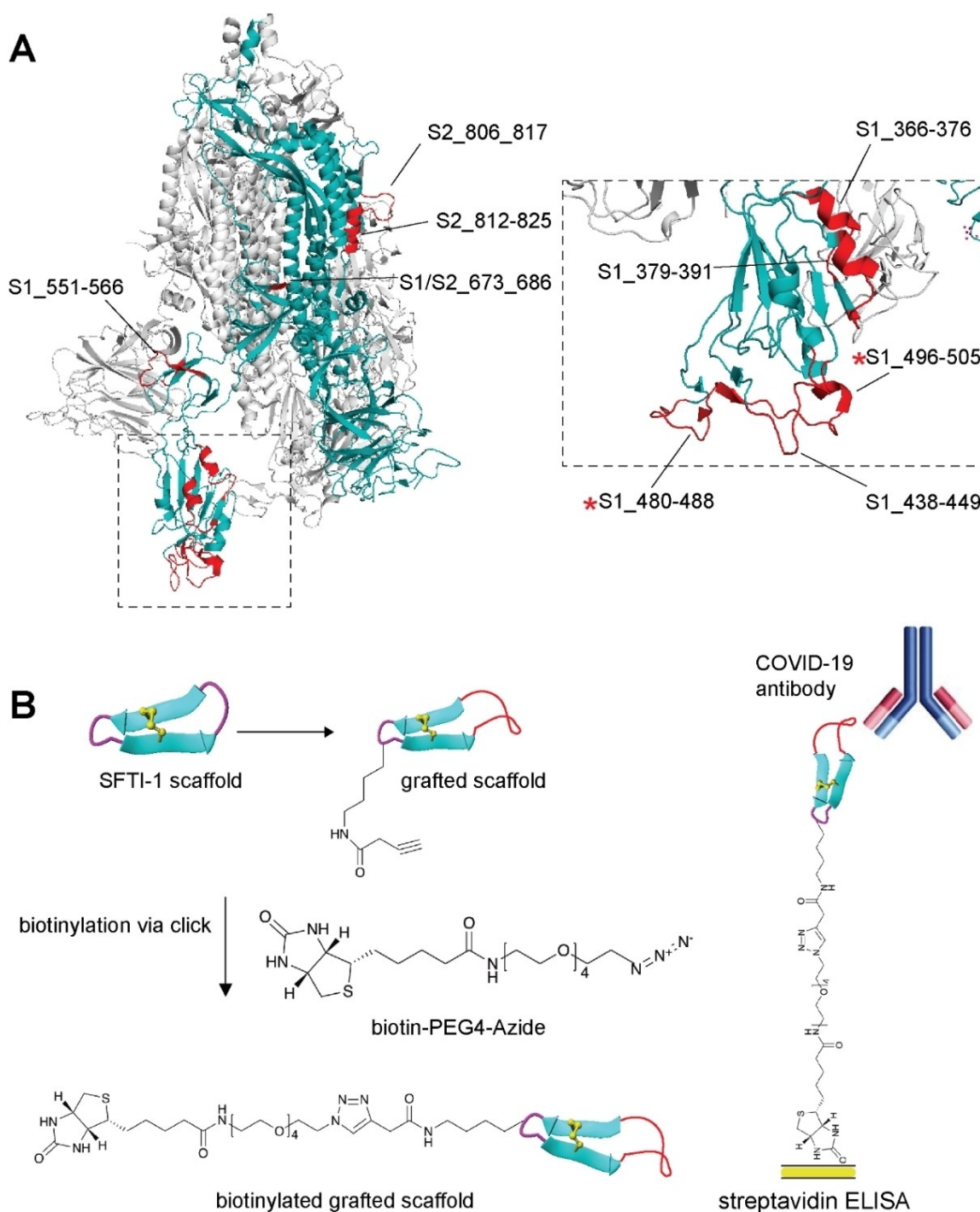


Figure 1. The concept of grafting. A) The structure to the left highlights one of the monomers of the spike protein trimer in cyan (PDB ID: 7DDN) with the epitopes selected for grafting marked in red. The receptor binding domain (RBD) is marked with a dashed square. The epitopes from the RBD are highlighted. Epitopes marked with an asterisk were combined to design the “double-loop peptide”, S1_477-508_I. The specific regions for S1_625-637 and S2_1148-1159 are missing in the available structure. For S1_673-686, only the first three starting residues are found in the available structure. B) In the grafting concept, an epitope (in red) from the spike protein is inserted into the scaffold peptide SFTI-1. The pentynoyl-lysine is incorporated into the primary loop. The peptide is biotinylated through click chemistry, in which a biotin-PEG4-azide is reacted with the pentynoyl-lysine alkyne side chain. The biotinylated peptide is then attached to streptavidin ELISA plates.

CTD) and from S2 (containing the fusion region and helical bundle proteins) and determined the binding to IgG antibodies in sera.

Results and Discussion

Selection of sequences/epitopes

Epitopes were selected based on the three-dimensional structure of the SARS-CoV-2 spike protein, with the hypothesis being that structures and sequences that reportedly are immunodominant and protrude from the core are more likely to be targeted by antibodies. Three loops of the RBD were identified as possible targets: S1_438-449, S1_480-488 and S1_496-505. Additional epitopes were selected based on the emerging literature on epitopes from immunodominant regions within the spike protein, reported to bind COVID-19 antibodies.^[38-48] This selection included epitopes from the C-terminal domain of S1 (S1_551-566), S1/S2 interface (S1_625-637), potential furin cleavage site (S1/S2_673-686), fusion protein region (S2_812-825), as highlighted in Fig 1. In addition, the heptad repeat region 2 (S2_1148-1159). Peptide sequences, their origin, and their molecular masses are shown in Table 1.

Synthesis of peptides

Selected epitopes were synthesized as both linear and cyclic peptides (i.e., grafted into the peptide scaffold SFTI-1, in place of its trypsin inhibitory loop). For the initial assay development, peptides were synthesized as C-terminal amides as the only modification. Later, all peptides were synthesized with a side-chain alkyne group (through a pentynoyl lysine in the cyclic peptides and an N-terminal propargyl-glycine in the linear peptides) to allow for biotinylation through click chemistry. The latter strategy allows for absolute selective labelling and control of the point of immobilization.

Peptides intended for cyclization were assembled by Fmoc-SPPS on the diamino benzoic acid (Dbz)-linked Dawson resin. The C-terminal Dbz thioester was converted to *N*-acyl-benzimidazolone (Nbz) prior to cyclization. At the N-terminal, a Boc-cysteine was introduced, which together with the Nbz group facilitates head-to-tail cyclization via native chemical ligation. The Boc cysteine also prevent modification by *para*-nitrochloroformate during Nbz conversion. All linear peptides were designed to contain a free N-terminal and an amidated C-terminal. For linear peptides intended for streptavidin ELISA, a propargyl-glycine was introduced at the N-terminal to enable subsequent biotinylation. The cyclic peptides intended for passive binding ELISA were synthesized with the sequence FPDGR in the secondary loop. In the case of cyclic peptides intended for streptavidin ELISA, the arginine in the secondary loop was replaced with a pentynoyl-Lys to facilitate subsequent biotinylation.

Table 1. Peptide sequences used for the development of SARS-CoV-2 ELISA.

Peptide name	Peptide sequence	Expected mass (M+H) ⁺ (monoisotopic)	Observed mass (M+H) ⁺ (monoisotopic)	Structural domain	Epitope REF
S1_366-376_l	GSVLYNSASFST-NH ₂	1269.35	1269.69	RBD	47
S1_379-391_l	----GCVGSPTKLNLC-NH ₂	1504.72	1505.81	RBD	38
S1-379-391_c	CFPDGKCYGVSPKLNLC-	2017.32	2017.04*		
S1_438-449_l	-----GSNNLDSKVGNGY-NH ₂	1361.41	1361.73	RBD	38
S1_438-449_c	CFPDGKCSNNLDSKVGNGY	2078.27	2078.03*		
S1_477-508_l	GSTPCNGVEGFNCYFPLQSYGFQPTNGVGYQP Y-NH ₂	3627.91	3627.43*	RBD	38,55
S1_480-488_l	----GCVGVEGFNC-NH ₂	1036.14	1035.45	RBD	
S1_480-488_c	CFPDGKCVGVEGFNC-	1547.01	1548.72*		
S1_496-505_l	----GQFQPTNGVGY-NH ₂	1133.20	1133.61	RBD	38
S1_496-505_c	CFPDGKCGFQPTNGVGY	1850.16	1850.88		
S1_551-566_l	----GVLTESNKKFLPFQQFG-NH ₂	1977.26	1977.20	C-terminal S1	43,44
S1_551_566_c	CFPDGKCVLTESNKKFLPFQQFG	2693.68	2693.44*		
S1_625-637_l	-----GHADQLTPTWRVYS-NH ₂	1668.81	1667.92	C-terminal S1	40,47
S1_623-639_c	CFPDGKCAIHADQLTPTWRVYSTG	2726.65	2726.41*		
S1/S2_673-686_l	GSYQTQTNSPRRARS-NH ₂	1745.85	1746.99*	S1/S2 interface	40,45
S2_806-817_l	GLPDPSKPSKRSF-NH ₂	1452.65	1452.89	FP	40
S2_812-825_l	-----GPSKRSFIEDLLFNK-NH ₂	1788.05	1788.12*	FP	40
S2_810-827_c	CFPDGKCSKPSKRSFIEDLLFNKVT	2919.85	2919.64*	FP	
S2_1148-1159_l	-----GFKEELDKYFKNH-NH ₂	1691.87	1691.94	HR2	40
S2_1146-1161_c	CFPDGKCSFKEELDKYFKNHTS	2798.62	2798.34*		

Mono.; monoisotopic, _l denotes linear peptides, _c denotes cyclic peptides. Propargyl-glycines are marked in blue. Pentynoyl-lysines are marked in red. Cysteine residues forming a disulfide bridge are marked in yellow. *: deconvoluted from (M+2H)²⁺ masses. RBD; receptor binding domain, FP; fusion peptide, HR; heptad repeat.

Dbz peptides were efficiently converted to Nbz peptides (no unconverted peptides were observed). Nbz peptides were then cleaved from the resin with TFA, simultaneously removing side-chain protection groups and the Boc group at the N-terminal cysteine, freeze-dried and subjected to cyclization. Notably, the alkyne side chain on the SARS-CoV-2 peptides remained intact and unreactive throughout Nbz conversion and cyclization reactions. The cyclic peptides were incubated in ammonium bicarbonate buffer overnight to ensure the formation of the disulfide bond. Peptides were isolated by RP-HPLC, and the purity of all peptides was >90% as judged by RP-HPLC-UV (215 nm). Identity of peptides was confirmed by mass spectrometry (Table 1).

Peptide biotinylation by click chemistry

Peptides were biotinylated through click chemistry, that is biotin was connected to the peptide through a 1,2,3-triazole linkage created by Cu^I catalysis of a 1,3-dipolar cycloaddition of an alkyne with an azide.^[49–51] First, peptide containing the alkyne was mixed with biotin-PEG4-azide. A solution of CuSO₄ containing Cu^{II} in complex with the chelating agent tris(3-hydroxypropyl)triazolylmethylamine (THPTA) was then introduced. Water-soluble THPTA allowed the entire click reaction to be carried out in aqueous medium. Addition of sodium ascorbate initiated the reduction of Cu^{II} to Cu^I, the catalyst for the click reaction which became evident by the blue-colored solution turning colorless. The presence of THPTA together with CuSO₄ ensured the stability of Cu^I to catalyze the click reaction which was complete within ~30 min. The oxidation of Cu^I back to Cu^{II} by dissolving oxygen in the click mixture was visible by the solution returning to blue color after ~30 min. Following the click reaction, the biotinylated peptide was obtained as one of the main products, however, unconjugated biotin-PEG4-azide, as well as unconjugated alkyne containing peptide could be detected in the solution mixture. Biotinylated peptides were purified by RP-HPLC (purity >90%) and used in the streptavidin ELISA. Representative mass spectra before and after biotinylation and chromatogram of the peptide S2_1146-1161_c is shown in Figure S1 in the Supporting Information.

Development of epitope-based SARS-CoV-2 ELISA

Initially, Maxisorp plates (high-binding capacity, recommended for use with Igs, binding capacity 600–650 ng IgG/cm³) were used to passively bind linear peptide amides. However, this setup gave high background and weak signals when tested within a range of coating concentrations, and the signal did not correlate with peptide concentration. We then used streptavidin-coated plates and biotinylated peptides. This improved the signal, which now correlated with peptide concentration, but the issue of high background (nonspecific binding) remained. In further optimization steps, several checkerboard titration assays were performed to determine the best conditions. First, the following 96-well plates were compared: Pierce™ streptavidin-

coated plate, clear, Pierce™ streptavidin-coated high sensitivity plate, clear, Pierce™ Streptavidin-coated high-capacity plate and Pierce™ neutravidin coated plate, clear. The streptavidin-coated high-capacity plate gave a higher signal-to-noise ratio and was selected for use with these peptides. All results from the comparison are shown in Figure S2.

To determine the optimal coating concentration, peptides S1_438-449_I, S1_379-391_I, S1_496-505_I and S1_480-488_I were chosen as test antigens. Peptides in concentrations from 10 to 0.625 µg/mL (using twofold dilutions) and one positive and one negative serum sample (serostatus was determined by lateral flow fast test) was added at 1:100, 1:200 and 1:400 dilution ratios. A peptide concentration of 5 µg/mL gave a superior signal-to-noise ratio and was therefore used in all ELISAs. Results from the peptide concentration checkerboard assay are shown in Figure S3. To assess what serum dilution factor was optimal, a plate was coated with a set peptide concentration determined from earlier titration experiments. Serum samples were diluted twofold from 1:50 (serum: buffer) to 1:3200 and applied to the plate. Peptide-coated wells with no serum added, and uncoated wells with serum added were used as controls. Serum dilution 1:100 was chosen as the best dilution factor.

To further reduce nonspecific binding, several blocking buffers were tested, including PBS with different concentrations of BSA and/or casein, with and without Tween-20, and commercial blocking buffers (Chonblock, Superblock, and Protein-free T20). Protein-free T20 blocking buffer resulted in the highest signal-to-noise ratio and was thereafter used in all experiments. The comparison is shown in Figure S4.

A checkerboard titration assay was then carried out to select conjugate concentration and serum dilution. Serum was diluted 1:100 (conjugate: buffer) to 1:3200, and the conjugate was diluted twofold from 1:5000 to 1:80000. The highest signal-to-noise ratio was obtained with 1:100 serum dilution with 1:5000 conjugate dilution. Finally, sample and substrate incubation time and temperature were tested. Coating at 25 °C for two hours was compared with 4 °C coating overnight. The latter gave higher signals and was therefore applied. For serum incubation, 30 min at 25 °C was compared with 30 min at 37 °C; the latter was the best option. For substrate incubation time, stop solution was added after 5, 10, 15, and 30 min. 15 min was chosen as the optimal reaction stop time.

Optimal conditions were used in all experiments described below and they are described in detail in the Experimental Section.

Application of in-house SARS-CoV-2 peptide ELISA and comparison of human SARS-CoV-2 spike trimer ELISA

The optimized ELISA was then used to test a cohort of 24 samples. The same cohort was tested using the Invitrogen human SARS-CoV-2 spike trimer total Ig ELISA according to manufacturer's recommendation, and all serum samples had been previously tested in a lateral flow fast test using Zhejiang Orient Gene Biotech SARS-CoV2 IgG/IgM rapid test. Pre-COVID-

19 sera were used to establish a cut-off value to distinguish between negative and positive samples.

Figure 2A compares the in-house ELISA and the commercial human spike trimer ELISA. In addition, samples positive in the lateral flow fast test are highlighted in red. Using the in-house ELISA, 14 of 24 serum samples were positive for the RBD positive control. In comparison, five out of 22 samples were positive in the spike trimer ELISA (two samples were not tested because of sample limitations), and eight in the lateral fast test. The five positives in the spike trimer ELISA were tested positive also in the lateral flow fast test and the in-house ELISA. Native scaffold peptide, SFTI-1, was used as negative control. No sample tested positive for that negative control, demonstrating that the scaffold itself was inert.

Binding to peptide epitopes, linear and in scaffold, varied substantially. Some peptides showed no binding, including linear and cyclic peptides containing epitopes S1_379-391, S1_438-449 S1_480-488, neither did the linear epitope S1/S2_673-686. On the contrary, peptides S1_477-508 and S2_810-827_c showed binding to all samples. Hence, none of these peptides appear to have any diagnostic value in this assay.

For epitopes S1_496-505 and S1_551-566, linear and cyclic peptides showed slight differences. Cyclic S1_496-505_c appeared to bind additional samples than the linear epitope, but those samples have tested negative in other assays. The same was the case for S1_551-566. Notably, individual sample reactivity may show high differences between linear and cyclic S1_551-566.

Epitope S1_625-637 and S2_812-825 show overall higher activity for cyclic peptides than linear ones. This includes an increase in reactivity of all samples tested positive in other assays, but sensitivity (i.e., the number of apparent false positives) of these peptides is inadequate.

The cyclic peptide S2_1146-1161_c appears to have the best diagnostic value under these assay conditions. This peptide contains four additional residues in the cyclic scaffold version compared with the linear S2_1148-1159_I. The linear epitope had a response frequency of 69% in a cohort of 1051 patients and epitope S2_1146-1166 was identified as an immunogenic region through VirScan and detected clear responses to COVID-19 patients.^[52] Six serum samples tested positive for S2_1146-1161_c. In comparison, five samples tested positive using commercial spike trimer ELISA; four of these were the same samples. Compared to the lateral flow assay, five out of the six positive samples also tested positive in that assay.

The UpSet plot in Figure 2B summarizes the reactivity between the best five antigens used in the current ELISA, based on the reactivity of the five samples that were positive in both the lateral flow test and the commercial human spike trimer ELISA. S2_1146-1161_c is among them, which also had the best selectivity as described above.

Notably, the epitopes originating from the RBD show no or little reactivity. If this is a result of the selection and design or mere absence of antibodies targeting these epitopes is unknown, but it can be noted that no epitopes that bind have yet been described from the RBD.^[43,53] However, it is clear that cyclization per se changes reactivity, when comparing all

samples towards linear and scaffold peptides (Figure S5). The current results also show some promise for epitope mapping, not the least from the results of S2_1146-1161_c.

Conclusions

In this work, we have shown the development of a SARS-CoV-2 ELISA. A series of optimization steps were required, with the way of binding of antigen to the plate and choice of blocking buffer being the most important steps. Twenty linear and grafted peptides were tested against SARS-CoV-2 serum samples, and large differences between them and between linear and grafted counterparts were demonstrated. One peptide showed performance comparable to that of commercial spike trimer ELISA, showing proof of concept.

Experimental Section

Reagents and materials: Pierce™ Streptavidin coated high-capacity plates (article no: 15500), TMB single solution ELISA (article no: 10445723), Pierce™ protein-free T20 (PBS) blocking buffer (article no: 10147483) were all from Fisher Scientific, Waltham, MA. ELISA stop solution (article no: 11652159) and ELISA wash buffer (article no: 15566266) were purchased from Invitrogen, Waltham, MA. Biotin-S-protein RBD (article no: ACRBSPDC82E925UG) was acquired from Acrobiosystems, Newark, DE. Reagents used for optimization: Blocker BSA (10X) in PBS (article no: 10341944) was from Thermo-Fisher Scientific, Göteborg, Sweden. Casein sodium salt and Tween-20 were both from Sigma-Aldrich, Steinheim, Germany. Chonblock blocking/sample dilution buffer (article no: CHO-9068) was from Hölzel-Diagnostika, Köln, Germany. SuperBlock (PBS) blocking buffer (article no: 13434299) was purchased from Thermo-Fisher Scientific. Microplates used for optimization were Pierce™ streptavidin-coated plates, clear, 96-Well (article no: 10485005), Pierce™ streptavidin-coated high-sensitivity plates, clear, 96 wells (article no:15520), Pierce™ neutravidin-coated plates, clear, 96-wells (article no: 15129) were all from Thermo-Fisher Scientific. Human SARS-CoV-2 Spike (Trimer) Ig total ELISA Kit was from Invitrogen. Phosphate-buffered-saline (PBS) was from Sigma-Aldrich. All Fmoc-amino acids, *N,N*-diisopropylethylamine (DIPEA), 3-[Bis(dimethylamino)methyl]methyl-3*H*-benzotriazol-1-oxide hexafluorophosphate (HBTU), triisopropylsilane (TIPS) and trifluoroacetic acid (TFA) were purchased from Iris Biotech (Germany). Acetonitrile (AcN), dichloromethane (DCM), guanidine hydrochloride (GuHCl), and diethyl ether were from VWR, Radnor, CA. Dimethylformamide (DMF) was from Honeywell, Germany. 3,4-diaminobenzoic acid (Dbz) was from AnaSpec, Fremont, CA. Tris(2-carboxyethyl)phosphine hydrochloride (TCEP-HCl) was from Iris Biotech, Marktredwitz, Germany. Piperidine, 4-mercaptophenylacetic acid (MPAA), formic acid (FA) and 4-nitrophenyl chloroformate were from Sigma-Aldrich, Steinheim, Germany. Disodium phosphate dibasic and sodium hydroxide were from Merck, Darmstadt, Germany. Ammonium hydrogen carbonate was from Fluka Chemie, Buchs, Switzerland. PEG4-azide was from Broadpharm, San Diego, CA. Tris(3-hydroxypropyl)triazolyl(methyl)amine (THPTA), Copper(II)sulfate, anhydrous, powder, and (+)-sodium L-ascorbate were from Scientific Laboratory Supplies, Nottingham, United Kingdom.

Peptide synthesis: Peptides were synthesized by using solid-phase peptide synthesis (SPPS) with Fmoc/*t*Bu orthogonal protection strategy, using 20% piperidine in DMF as the deprotecting agent

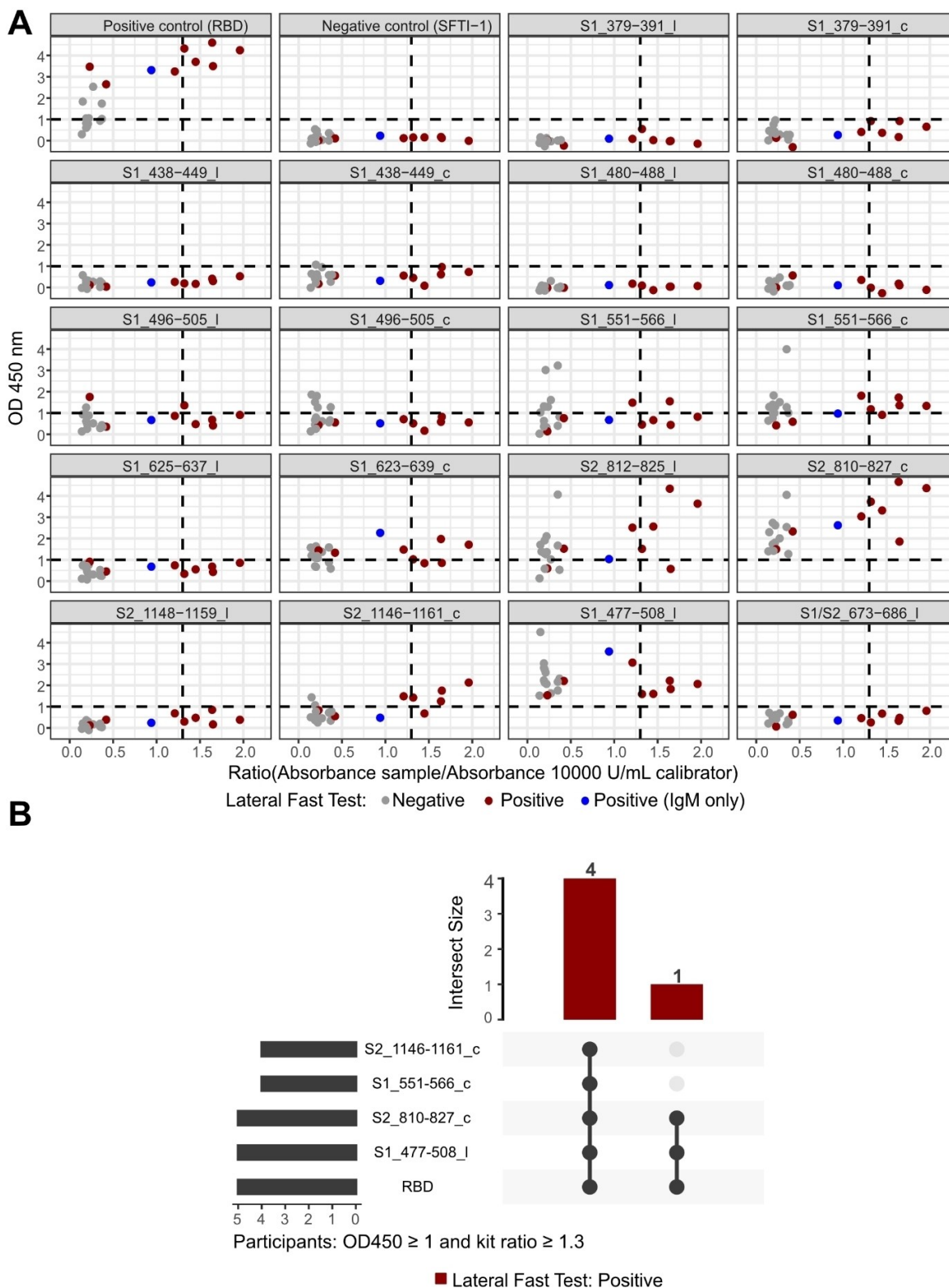


Figure 2. A) A comparison between our developed indirect in-house SARS-CoV-2-ELISA (shown epitope by epitope) and commercial human SARS-CoV-2 spike trimer total Ig ELISA. The mean response plus three times the standard deviation of negative control (pre-covid outbreak SLE patient sera) was used as a cut-off value for positivity. Thus, serum samples with a reactivity $>$ 1 were deemed positive, while sera with a reactivity $<$ 1 were deemed negative. Cut-off values for positivity are shown as dotted lines (cut-off for positivity was an absorbance value of 1 and an absorbance ratio 1.3). The numbers of positive sera in the separate assays are summarized in the Supporting Information Table 1. B) UpSet plot summarizing the top five antigens among individuals that passed the set cut-off limit. All five individuals scored positive on the lateral flow fast test.

and HBTU/DIPEA for amino acid coupling. The peptides were either synthesized manually or with a microwave-assisted automatic synthesizer (Liberty 1, CEM, Matthews, NC).

Linear peptide synthesis: Linear epitopes were assembled using manual synthesis on tentagel rink amide resin (scale 0.1 mmol, substitution value 0.19 mmol/g). All amino acids were added in 4 equiv. excess (relative to resin), as was coupling reagent HBTU in DMF, while DIPEA was added at 6 equiv. excess. An N-terminal propargyl glycine was coupled to the peptides that were intended for streptavidin ELISA. The N-terminal Fmoc group was removed (deprotection time was 20 min) and the peptides were cleaved from the resin and side-chain protection groups using TFA/TIPS/water (95:2.5:2.5, v/v/v), 10 mL of cleavage mixture for 100 mg of resin).

Cyclic peptide synthesis: Cyclic peptides were assembled on Dawson Dbz resin (substitution value: 0.4 mmol/g, Novabiochem, VWR, Radnor, CA) on a 0.1 mmol scale. The first two to three C-terminal residues were coupled manually at room temperature (RT) while the remaining residues (up to Fmoc-pentynoyl-lysine) were coupled using automatic microwave-assisted synthesis, using a method we have described previously^[54]. Fmoc-pentynoyl-lysine and the rest of the amino acids up to the N-terminal were coupled manually. Fmoc-pentynoyl-Lys-OH was coupled at 2 equiv. of resin, 2 equiv. of HBTU and 4 equiv. of DIPEA. A Boc-Cys was introduced at the N-terminal to protect the N-terminal during cyclization steps. Following washing and drying of the resin-peptide, an on-resin conversion from Dbz peptide to NBZ-peptide (*N*-benzylimidazolone) was performed using 16 equiv. of 4-nitrochloroformate for 1 h ($\times 2$), stirring. The resin was washed thoroughly with DMF and 195 equiv. of DIPEA in DMF was added to the resin and stirred well for 25 min. Resin was washed thoroughly with DCM and dried under N_2 gas. Simultaneous cleavage from resin and protection groups was performed through the addition of (TFA/TIPS/water 95:2.5:2.5, v/v/v) 10 mL per 100 g of resin. Cleaved Nbz peptide was precipitated with cold diethyl ether and collected by centrifugation. After freeze drying, the resulting NBZ peptides (25–30 mg) were cyclized in 0.159 M sodium phosphate ($Na_2HPO_4 \cdot 2H_2O$), 6 M GuHCl, 50 mM mercaptophenyl acetic acid (MPAA) and 20 mM TCEP. The pH of the reaction was adjusted to 7.1–7.2. The solution was kept stirring overnight at room temperature. The cyclic peptide was collected by size-exclusion chromatography using a Sephadex G-25 column. After freeze drying the peptides were subjected to oxidative folding (0.1 M NH_4HCO_3 buffer, pH 8.5, for 24 h). Following oxidation, peptides were purified by RP-HPLC and the purity was assessed by analytical HPLC-UV and MS.

Click chemistry: A solution of 100 mM $CuSO_4$ in 200 mL Milli-Q water was prepared and mixed with a solution of 200 mM tris(3-hydroxypropyltriazolylmethyl)amine (THPTA) in Milli-Q water (200 mL) in a ratio of 1:1 (v/v). The THPTA solution was aliquoted (100 mL/aliquot) and stored at $-20^\circ C$. 12.5 equiv. of 10 mM biotin-PEG4-azide were dissolved in 10% DMSO (and 90% water). To this solution, 25 equiv. of THPTA/ $CuSO_4$ solution was added together with 25 equiv. to ~ 1 mg of the purified alkyne-containing peptide. After vortexing, 40 equiv. of 100 mM sodium ascorbate in water was added to initiate the biotin click reaction (stirring RT for ~ 30 min). The solution was purified using a 0.3 mL/min gradient on RP-HPLC.

Serum samples: Informed consent was obtained from all participants before serum samples were collected. Human serum collection was approved by Uppsala (healthy donors, DNR 2018/206) and Stockholm (SLE patients pre-COVID, DNR 2015/2001-31/2) regional ethical committees. Serological lateral flow fast tests were performed using the COVID-19 IgG/IgM rapid test cassette

(Zhejiang Orient Gene Biotech Co Ltd, Huzhou, Zhejiang, China) according to the manufacturer's instructions (not done on pre-COVID samples). All samples for our work were anonymous.

In-house SARS-COV-2 peptide ELISA: Pierce™ streptavidin-coated high capacity 96-well plates (Fischer Scientific, 15500) were pre-washed with 3 \times 300 μL coating buffer (PBS; 0.01 M phosphate, 0.154 M NaCl supplied with 0.05% Tween 20). Biotinylated peptides and biotinylated RBD were dissolved in a coating buffer to a concentration of 5 $\mu g/mL$. 100 μL was added to most wells, whereas other wells were subjected to antigen-free coating buffer to serve as controls for nonspecific binding. The plates were incubated overnight at $4^\circ C$. The wells were washed three times with ELISA wash buffer (Invitrogen) 300 $\mu L/well$ and blocked with 300 $\mu L/well$ Pierce™ Protein-Free T20 for 30 min at room temperature. The wells were emptied from the buffer. Serum samples and serum control samples were diluted 1:100 in blocking buffer and directly added to the plate (100 $\mu L/well$). The plates were incubated at $37^\circ C$ for 60 min. The wells were washed four times and incubated with goat-anti-human antibody-HRP conjugate in blocking buffer (1:5000, 100 $\mu L/well$) for 30 min at $37^\circ C$. Following four washes, 100 $\mu L/well$ of TMB substrate was added and the plates were incubated in the dark at RT for 15 min. The enzymatic reaction was quenched using 100 $\mu L/well$ of ELISA stop solution and absorbance at 450 nm was read immediately on a Varioskan spectrophotometer.

Human SARS-COV-2 spike (trimer) Ig total ELISA: All serum samples were subjected to a commercial SARS-CoV-2 Ig ELISA; human SARS-CoV-2 spike (trimer) Ig total ELISA Kit (Invitrogen, BMS2323). The ELISA plate was washed 2 times in 1x wash buffer and 90 μL 1x assay buffer was added to all wells except blanks (100 μL) and standards (0 μL). 100 μL of standard samples at 40000, 10000, and 2500 U/mL were added to control wells. Serum samples were diluted in 1x Assay buffer to a concentration of 1:100 and 10 μL of each sample was added to all wells (except those for blanks and standards). The plate was incubated at $37^\circ C$ for 30 min and washed three times with 1x wash buffer. HRP-conjugate (100 $\mu L/well$) was added and incubated at $37^\circ C$ for 30 min. All wells were washed three times and 100 $\mu L/well$ of substrate solution was added and incubated for 15 min at RT. Stop solution (100 $\mu L/well$) was added and absorbance was read at wavelength 450 nm on a Varioskan spectrophotometer. In the human SARS-CoV-2 spike trimer ELISA, sample absorbance was compared qualitatively to the 10000 U/mL standard (Absorbance sample/Absorbance 10000 U/mL calibrator). According to the kit protocol, ratios > 1.3 were determined positive, 1–1.3 undetermined and ratios < 1 negative.

Acknowledgements

The study was supported by SciLifeLab National COVID-19 Research Program and the Knut and Alice Wallenbergs Stiftelse (KAW 2020.0182). Work on peptide scaffolds in the Göransson lab is supported by the Swedish Research Council (2018-03318). We thank Jay Persson and Sara Joher for assistance with peptide synthesis.

Conflict of Interests

The authors declare no conflict of interest.

Data Availability Statement

The data that support the findings of this study are available from the corresponding author upon reasonable request.

Keywords: ELISA · epitopes · SARS-CoV-2 · scaffold peptides · SFTI-1

- [1] J. F. W. Chan, S. Yuan, K. H. Kok, K. K. W. To, H. Chu, J. Yang, F. Xing, J. Liu, C. C. Y. Yip, R. W. S. Poon, H. W. Tsoi, S. K. F. Lo, K. H. Chan, V. K. M. Poon, W. M. Chan, J. D. Ip, J. P. Cai, V. C. C. Cheng, H. Chen, C. K. M. Hui, K. Y. Yuen, *Lancet* **2020**, *395*, 514–523.
- [2] C. Wang, P. W. Horby, F. G. Hayden, G. F. Gao, *Lancet* **2020**, *395*, 470–473.
- [3] C. Huang, Y. Wang, X. Li, L. Ren, J. Zhao, Y. Hu, L. Zhang, G. Fan, J. Xu, X. Gu, Z. Cheng, T. Yu, J. Xia, Y. Wei, W. Wu, X. Xie, W. Yin, H. Li, M. Liu, Y. Xiao, H. Gao, L. Guo, J. Xie, G. Wang, R. Jiang, Z. Gao, Q. Jin, J. Wang, B. Cao, *Lancet* **2020**, *395*, 497–506.
- [4] A. A. Rabaan, S. H. Al-Ahmed, S. Haque, R. Sah, R. Tiwari, Y. S. Malik, K. Dhama, M. I. Yatoo, D. K. Bonilla-Aldana, A. J. Rodriguez-Morales, *Infez. Med.* **2020**, *28*, 174–184.
- [5] P. Zhou, X. Lou Yang, X. G. Wang, B. Hu, L. Zhang, W. Zhang, H. R. Si, Y. Zhu, B. Li, C. L. Huang, H. D. Chen, J. Chen, Y. Luo, H. Guo, R. Di Jiang, M. Q. Liu, Y. Chen, X. R. Shen, X. Wang, X. S. Zheng, K. Zhao, Q. J. Chen, F. Deng, L. L. Liu, B. Yan, F. X. Zhan, Y. Y. Wang, G. F. Xiao, Z. L. Shi, *Nature* **2020**, *579*, 270–273.
- [6] C. Drosten, S. Günther, W. Preiser, S. van der Werf, H.-R. Brodt, S. Becker, H. Rabenau, M. Panning, L. Kolesnikova, R. A. M. Fouchier, A. Berger, A.-M. Burguère, J. Cinatl, M. Eickmann, N. Escρίου, K. Grywna, S. Kramme, J.-C. Manuguerra, S. Müller, V. Rickerts, M. Stürmer, S. Vieth, H.-D. Klenk, A. D. M. E. Osterhaus, H. Schmitz, H. W. Doerr, *N. Engl. J. Med.* **2003**, *348*, 1967–1976.
- [7] T. G. Ksiazek, D. Erdman, C. S. Goldsmith, S. R. Zaki, T. Peret, S. Emery, S. Tong, C. Urbani, J. A. Comer, W. Lim, *N. Engl. J. Med.* **2020**, *348*, 1953–1966.
- [8] F. Li, *Annu. Rev. Virol.* **2016**, *3*, 237–261.
- [9] S. Satarker, M. Nampoothiri, *Arch. Med. Res.* **2020**, *51*, 482–491.
- [10] C. B. Jackson, M. Farzan, B. Chen, H. Choe, *Nat. Rev. Mol. Cell Biol.* **2022**, *23*, 3–20.
- [11] S. Jiang, C. Hillyer, L. Du, *Trends Immunol.* **2020**, *41*, 355–359.
- [12] Z. Zhu, S. Chakraborti, Y. He, A. Roberts, T. Sheahan, D. Xiao, L. E. Hensley, P. Prabhakaran, B. Rockx, I. A. Sidorov, O. Corti, L. Vogel, Y. Feng, J. O. Kim, L. F. Wang, R. Baric, A. Lanzavecchia, K. M. Curtis, G. J. Nabel, K. Subbarao, S. Jiang, D. S. Dimitrov, *Proc. Natl. Acad. Sci. USA* **2007**, *104*, 12123–12128.
- [13] R. A. Perera, C. K. Mok, O. T. Tsang, H. Lv, R. L. Ko, N. C. Wu, M. Yuan, W. S. Leung, J. M. Chan, T. S. Chik, C. Y. Choi, K. Leung, K. H. Chan, K. C. Chan, K.-C. Li, J. T. Wu, I. A. Wilson, A. S. Monto, L. L. Poon, M. Peiris, *Eurosurveillance* **2020**, *25*, 1–9.
- [14] F. Amanat, T. Nguyen, V. Chromikova, S. Strohmeier, D. Stadlbauer, A. Javier, K. Jiang, G. Asthagiri-Arun Kumar, J. Polanco, M. Bermudez-Gonzalez, D. Caplinski, A. Cheng, K. Kedzierska, O. Vapalahti, J. Hepojoki, V. Simon, F. Krammer, *Nat. Med.* **2020**, *26*, 1033–1036.
- [15] S. N. Amrun, C. Y. P. Lee, B. Lee, S. W. Fong, B. E. Young, R. S. L. Chee, N. K. W. Yeo, A. Torres-Ruesta, G. Carissimo, C. M. Poh, Z. W. Chang, M. Z. Tay, Y. H. Chan, M. I. C. Chen, J. G. H. Low, P. A. Tambayah, S. Kalimuddin, S. Pada, S. Y. Tan, L. J. Sun, Y. S. Leo, D. C. Lye, L. Renia, L. F. P. Ng, *EBioMedicine* **2020**, *10.1016/j.ebiom.2020.102911*.
- [16] S. Gunasekera, F. M. Foley, R. J. Clark, L. Sando, L. J. Fabri, D. J. Craik, N. L. Daly, *J. Med. Chem.* **2008**, *51*, 7697–7704.
- [17] D. J. Craik, N. L. Daly, T. Bond, C. Waine, *J. Mol. Biol.* **1999**, *294*, 1327–1336.
- [18] A. G. Poth, L. Y. Chan, D. J. Craik, *Biopolymers* **2013**, *100*, 480–491.
- [19] D. J. Craik, J. Du, *Curr. Opin. Chem. Biol.* **2017**, *38*, 8–16.
- [20] D. J. Craik, J. E. Swedberg, J. S. Mylne, M. Cemazar, *Expert Opin. Drug Discovery* **2012**, *7*, 179–194.
- [21] S. Luckett, R. S. Garcia, J. J. Barker, A. V. Konarev, P. R. Shewry, R. Clarke, R. L. Brady, *J. Mol. Biol.* **1999**, *290*, 525–533.
- [22] L. Y. Chan, S. Gunasekera, S. T. Henriques, N. F. Worth, S. J. Le, R. J. Clark, J. H. Campbell, D. J. Craik, N. L. Daly, *Blood* **2011**, *118*, 6709–6717.
- [23] C. K. Wang, S. E. Northfield, Y. H. Huang, M. C. Ramos, D. J. Craik, *Eur. J. Med. Chem.* **2016**, *109*, 342–349.
- [24] R. Sable, T. Durek, V. Taneja, D. J. Craik, S. Pallerla, T. Gauthier, S. Jois, *ACS Chem. Biol.* **2016**, *11*, 2366–2374.
- [25] Y. Qiu, M. Taichi, N. Wei, H. Yang, K. Q. Luo, J. P. Tam, *J. Med. Chem.* **2017**, *60*, 504–510.
- [26] A. C. Conibear, S. Chaouis, T. Durek, K. Johan Rosengren, D. J. Craik, C. I. Schroeder, *Biopolymers* **2016**, *106*, 89–100.
- [27] F. Zoller, A. Markert, P. Barthe, W. Zhao, W. Weichert, V. Askoxylakis, A. Altmann, W. Mier, U. Haberkorn, *Angew. Chem. Int. Ed.* **2012**, *51*, 13136–13139.
- [28] S. Roesch, T. Lindner, M. Sauter, A. Loktev, P. Flechsig, M. Müller, W. Mier, R. Warta, G. Dyckhoff, C. Herold-Mende, U. Haberkorn, A. Altmann, *J. Nucl. Med.* **2018**, *59*, 1679–1685.
- [29] S. Gunasekera, C. Fernandes-Cerqueira, S. Wennmalm, H. Wähämaa, Y. Sommarin, A. I. Catrina, P. J. Jakobsson, U. Göransson, *ACS Chem. Biol.* **2018**, *13*, 1525–1535.
- [30] L. Y. Chan, D. J. Craik, N. L. Daly, *Biosci. Rep.* **2015**, *35*, 1–12.
- [31] L. Y. Chan, D. J. Craik, N. L. Daly, *Sci. Rep.* **2016**, *6*, 1–13.
- [32] J. Zhang, S. Yamaguchi, T. Nagamune, *Biotechnol. J.* **2015**, *10*, 1499–1505.
- [33] C. C. Caceres, P. S. Bansal, S. Navarro, D. Wilson, L. Don, P. Giacomini, A. Loukas, N. L. Daly, *J. Biol. Chem.* **2017**, *292*, 10288–10294.
- [34] T. Durek, P. M. Cromm, A. M. White, C. I. Schroeder, Q. Kaas, J. Weidmann, A. Ahmad Fuaad, O. Cheneval, P. J. Harvey, N. L. Daly, Y. Zhou, A. Dellsén, T. Österlund, N. Larsson, L. Knerr, U. Bauer, H. Kessler, M. Cai, V. J. Hruby, A. T. Plowright, D. J. Craik, *J. Med. Chem.* **2018**, *61*, 3674–3684.
- [35] R. I. Lehrer, A. M. Cole, M. E. Selsted, *J. Biol. Chem.* **2012**, *287*, 27014–27019.
- [36] M. L. J. Korsinczyk, H. J. Schirra, K. J. Rosengren, J. West, B. A. Condie, L. Otvos, M. A. Anderson, D. J. Craik, *J. Mol. Biol.* **2001**, *311*, 579–591.
- [37] S. J. De Veer, S. S. Ukolova, C. A. Munro, J. E. Swedberg, A. M. Buckle, J. M. Harris, *Biopolymers* **2013**, *100*, 510–518.
- [38] Y. Chen, Y. Guo, Y. Pan, Z. J. Zhao, *Biochem. Biophys. Res. Commun.* **2020**, *525*, 135–140.
- [39] Y. Li, D. Y. Lai, H. N. Zhang, H. W. Jiang, X. Tian, M. L. Ma, H. Qi, Q. F. Meng, S. J. Guo, Y. Wu, W. Wang, X. Yang, D. W. Shi, J. B. Dai, T. Ying, J. Zhou, S. C. Tao, *Cell. Mol. Immunol.* **2020**, *17*, 1095–1097.
- [40] L. Farrera-Soler, J.-P. Daguer, S. Barluenga, P. R. Cohen, S. Pagano, S. Yerly, L. Kaiser, N. Vuilleumier, N. Winssinger, *PLoS One* **2020**, *15*, 10.1371/journal.pone.0238089
- [41] C. M. Poh, G. Carissimo, B. Wang, S. N. Amrun, C. Y. P. Lee, R. S. L. Chee, S. W. Fong, N. K. W. Yeo, W. H. Lee, A. Torres-Ruesta, Y. S. Leo, M. I. C. Chen, S. Y. Tan, L. Y. A. Chai, S. Kalimuddin, S. S. G. Kheng, S. Y. Thien, B. E. Young, D. C. Lye, B. J. Hanson, C. I. Wang, L. Renia, L. F. P. Ng, *Nat. Commun.* **2020**, *11*, 10.1038/s41467-020-16638-2.
- [42] V. Shivarov, P. K. Petrov, A. D. Pashov, *Front. Immunol.* **2020**, *11*, 1–5.
- [43] A. Grifoni, J. Sidney, Y. Zhang, R. H. Scheuermann, B. Peters, A. Sette, *Cell Host Microbe* **2020**, *27*, 671–680.e2.
- [44] B.-Z. Zhang, Y.-F. Hu, L.-L. Chen, Y.-G. Tong, J.-C. Hu, J.-P. Cai, K. H. Chan, Y. Dou, J. Deng, H.-R. Gong, C. Kuwantra, W. Li, X.-L. Wang, H. Chu, C.-h. Su, I. F.-N. Hung, T. C. C. Yau, K. K. W. To, K. Y. Yuen, J.-D. Huang, *Cell Res.* **2020**, *30*, 702–704, <https://doi.org/10.1038/s41422-020-0366-x>.
- [45] J. A. Jaimas, N. M. Andre, J. K. Millet, G. R. Whittaker, *ArXiv preprint* **2020**, 1–36.
- [46] E. Y. Wang, T. Mao, J. Klein, Y. Dai, J. D. Huck, F. Liu, S. Zheng, T. Zhou, B. Israelow, P. Wong, C. Lucas, J. Silva, J. E. Oh, E. Song, E. S. Perotti, S. Fischer, M. Campbell, B. John, A. L. Wyllie, C. B. F. Vogels, I. M. Ott, C. C. Kalinich, W. L. Schulz, N. D. Grubaugh, A. I. Ko, A. Iwasaki, A. Ring, *Nature* **2021**, *595*, 283–288, [10.1038/s41586-021-03631-y](https://doi.org/10.1038/s41586-021-03631-y).
- [47] Q.-D. Su, Y. Yi, Y.-N. Zou, Z.-Y. Jia, F. Qiu, F. Wang, W.-J. Yin, W.-T. Zhou, S. Zhang, P.-C. Yu, S.-L. Bi, L.-P. Shen, G.-Z. Wu, *Vaccine* **2020**, *38*, 5071–5075.
- [48] S. Mukherjee, D. Tworowski, R. Detroja, S. B. Mukherjee, M. Frenkel-Morgenstern, *Vaccine* **2020**, *8*, 1–17.
- [49] T. R. Chan, R. Hilgraf, K. B. Sharpless, V. V. Fokin, *Org. Lett.* **2004**, *6*, 2853–2855.
- [50] V. Hong, S. I. Presolski, C. Ma, M. G. Finn, *Angew. Chem. Int. Ed.* **2009**, *48*, 9879–9883.
- [51] F. Manzenrieder, R. Luxenhofer, M. Retzlaff, R. Jordan, M. G. Finn, *Angew. Chem. Int. Ed.* **2011**, *50*, 2601–2605.
- [52] Y. Li, M. L. Ma, Q. Lei, F. Wang, W. Hong, D. Y. Lai, H. Hou, Z. W. Xu, B. Zhang, H. Chen, C. Yu, J. B. Xue, Y. X. Zheng, X. N. Wang, H. W. Jiang, H. N. Zhang, H. Qi, S. Juan Guo, Y. Zhang, X. Lin, Z. Yao, J. Wu, H. Sheng, Y. Zhang, H. Wei, Z. Sun, X. Fan, S. C. Tao, *Cell Rep.* **2021**, *34*, 108915.

- [53] A. V. Wisnewski, C. A. Redlich, J. Liu, K. Kamath, Q. A. Abad, R. F. Smith, L. Fazen, R. Santiago, J. C. Luna, B. Martinez, E. Baum-Jones, R. Waitz, W. A. Haynes, J. C. Shon, *PLoS One* **2021**, *16*, 1–13.
- [54] S. Gunasekera, T. L. Aboye, W. A. Madian, H. R. El-Seedi, U. Göransson, *Int. J. Pept. Res. Ther.* **2013**, *19*, 43–54.
- [55] J. Dong, S. J. Zost, A. J. Greaney, T. N. Starr, A. S. Dingens, E. C. Chen, R. E. Chen, J. B. Case, R. E. Sutton, P. Gilchuk, J. Rodriguez, E. Armstrong, C. Gainza, R. S. Nargi, E. Binshtein, X. Xie, X. Zhang, P. Y. Shi, J. Logue, S. Weston, M. E. McGrath, M. B. Frieman, T. Brady, K. M. Tuffy, H. Bright,

Y. M. Loo, P. M. McTamney, M. T. Esser, R. H. Carnahan, M. S. Diamond, J. D. Bloom, J. E. Crowe, *Nat. Microbiol.* **2021**, *6*, 1233–1244.

Manuscript received: February 7, 2023
Revised manuscript received: April 3, 2023
Accepted manuscript online: April 6, 2023
Version of record online: July 12, 2023